Left ventricular strain and its pattern estimated from cine CMR and validation with DENSE

IOP Publishing | Institute of Physics and Engineering in Medicine Physics in Medicine and Biology

Phys. Med. Biol. **59** (2014) 3637–3656 doi:10.1088/0031-9155/59/13/3637

Left ventricular strain and its pattern estimated from cine CMR and validation with DENSE

Hao Gao[1], **Andrew Allan**[2], **Christie McComb**[2], **Xiaoyu Luo**[1] **and Colin Berry**[2,3]

[1] School of Mathematics and Statistics, University of Glasgow, Glasgow, G12 8QW, UK
[2] BHF Glasgow Cardiovascular Research Centre, University of Glasgow, Glasgow, G12 8TA, UK

E-mail: hao.gao@glasgow.ac.uk, Xiaoyu.luo@glasgow.ac.uk, a.allan.1@research.gla.ac.uk, christie.mccomb@nhs.net and colin.berry@glasgow.ac.uk

Received 11 September 2013, revised 13 December 2013
Accepted for publication 22 May 2014
Published 12 June 2014

Abstract

Measurement of local strain provides insight into the biomechanical significance of viable myocardium. We attempted to estimate myocardial strain from cine cardiovascular magnetic resonance (CMR) images by using a b-spline deformable image registration method. Three healthy volunteers and 41 patients with either recent or chronic myocardial infarction (MI) were studied at 1.5 Tesla with both cine and DENSE CMR. Regional circumferential and radial left ventricular strains were estimated from cine and DENSE acquisitions. In all healthy volunteers, there was no difference for peak circumferential strain (-0.18 ± 0.04 versus -0.18 ± 0.03, $p = 0.76$) between cine and DENSE CMR, however peak radial strain was overestimated from cine (0.84 ± 0.37 versus 0.49 ± 0.2, $p < 0.01$). In the patient study, the peak strain patterns predicted by cine were similar to the patterns from DENSE, including the strain evolution related to recovery time and strain patterns related to MI scar extent. Furthermore, cine-derived strain disclosed different strain patterns in MI and non-MI regions, and regions with transmural and non-transmural MI as DENSE. Although there were large variations with radial strain measurements from cine CMR images, useful circumferential strain information can be

[3] Author to whom any correspondence should be addressed.

obtained from routine clinical CMR imaging. Cine strain analysis has potential to improve the diagnostic yield from routine CMR imaging in clinical practice.

Keywords: myocardial strain, deformable image registration, DENSE, myocardial infarction

(Some figures may appear in colour only in the online journal)

1. Introduction

Cardiovascular magnetic resonance (CMR) imaging has emerged as a gold standard diagnostic method for *in vivo* assessment of heart disease and its functional significance (Berry *et al* 2010, Isbell and Kramer 2005). Myocardial strain, or deformation, reflects contractility (Leitman *et al* 2004) and measurements of local strain patterns by using CMR provide insights into the biomechanical significance of viable myocardium (Aletras *et al* 2011).

Myocardial strain estimated from dedicated CMR contains biomechanical information that is much more closely linked to contractility than displacement imaging with anatomical cine CMR. There are several CMR techniques for estimating strain including tagged CMR (Zerhouni *et al* 1988), cine phase-contrast velocity imaging (Jung *et al* 2006), strain-encoded CMR (Osman *et al* 2001) and displacement encoding with stimulated-echo (DENSE) (Aletras *et al* 1999). Each modality has advantages and disadvantages (Ibrahim el 2011). Tagged CMR is a validated tool for quantification of left ventricular (LV) strain from two-dimensional (2D) to 3D (Moore *et al* 2000). However, tagged CMR has some limitations including rather complex processing, low resolution (in radial direction), and difficulties in estimating strain in late diastole due to the fading of tag patterns (Li and Denney 2006, Xu *et al* 2010). Cine phase-contrast velocity imaging is also susceptible to artefacts related to tissue motion. The advantages of strain-encoded CMR include the short acquisition time, simple post-processing and high temporal resolution, however it measures strain only in the through-plane direction and does not permit motion tracking (Neizel *et al* 2009). DENSE is a recently developed technique which combines the advantages from both tagged CMR and cine phase-contrast velocity imaging with high spatial resolution (Wen *et al* 2008). It has also been validated against tagged CMR in phantom and clinical studies (Kim *et al* 2004). Using DENSE, myocardial strain can be estimated in longitudinal, circumferential and radial directions. Although DENSE is a promising research tool (Aletras *et al* 1999, Nasiraei Moghaddam *et al* 2010) it still requires separate breath-hold scans in addition to the standard cine CMR. The DENSE breath-holds are typically long (>15 s) which may be less well tolerated by infirm patients with breath-holding difficulties or may result in imperfect data due to respiratory motions (Kim and Kellman 2007).

Most clinical CMR laboratories do not estimate strain because of challenges in acquiring high quality strain data and estimating strain in post-processing. Since cine CMR is always performed to assess anatomy and function (Castillo *et al* 2003), innovative approaches to measure strain from cine scans are desirable. Techniques such as deformable methods and feature tracking have been developed for myocardial strain estimation based on cine CMR images (Veress *et al* 2005, Feng *et al* 2008, Mansi *et al* 2009, Hor *et al* 2010). There are mainly two types of deformable methods, one is the shape-based matching in which LV deformation is estimated by matching geometry features, such as curvature (Sinusas *et al* 2001) or corner points from images (Shi *et al* 2009). Sinusas *et al* (2001) quantified regional myocardial deformation during diastole in eight canines with cine CMR by using a 3D shape-based matching, which tracked the 3D trajectories of a field of points from endocardial and epicardial surfaces. Local myofibre strain was calculated using the finite element method under

linear and infinitesimal deformation assumptions. Papademetris *et al* (2002) applied a similar method to estimate myocardial deformation in open chest dogs before and after coronary occlusion. The estimated strains from the same animals were highly correlated to the values derived from implanted markers. Conti *et al* (2011) calculated strains with point tracking from cine CMR with a virtual heart phantom, and compared these data with strains from a finite element model. They found that local strains agreed well with the results from finite element modelling.

The second approach, also known as deformation registration, is to seek LV deformation by matching the image features, such as intensity and mutual information (Rueckert *et al* 1999). This approach involves deforming one image (target) into another image (reference) by minimizing a certain energy function, such as hyper-elastic warping with finite element representation of LV (Veress *et al* 2005, Phatak *et al* 2009), and non-rigid registration (Feng *et al* 2008, Rueckert *et al* 1999). Wierzbicki *et al* (2004) estimated the epicardial surface motion from an excised porcine heart with a non-rigid registration method, and validated the estimated motion with tracking of implanted fiducial markers. They also studied the dynamic heart motion with CT images of canine subjects, and with CMR images of human subjects. Their results suggested that the non-rigid registration method could track the heart motion well with appropriate similarity metrics, especially for the epicardial surface. However, the accuracy of estimated strains from the non-rigid registration method was not evaluated. Bistoquet *et al* (2007) used an incompressible model to estimate LV strain by matching the mid-surface of the left ventricle and maximizing mutual information. The recovered LV wall deformation and strains agreed well with tagged CMR scans. Veress *et al* (2005) developed a hyper-elastic warping method for LV strain during diastole by using cine CMR from a healthy volunteer, and compared the strain data with results from a finite element model. They used image intensity differences from the reference and target images to generate a body force to deform a finite element representation of the reference image so that the two images could be aligned. Later, the work was extended to estimate LV strain in systole (Phatak *et al* 2009), and validated with tagged CMR. They demonstrated that deformable image registration method could be an alternative method for quantifying regional LV deformation. However, one limitation was that their models required information on detailed myofibre structure, which is difficult to obtain *in vivo*.

The methods for 3D LV strain estimation from cine CMR require complex modelling techniques and imaging processing (Veress *et al* 2005, Conti *et al* 2011). Accordingly, 2D based LV strain estimation from cine CMR could be more applicable in a clinical setting provided there is adequate diagnostic limited accuracy for circumferential, radial and longitudinal strains. By using 2D strain analysis, Hor *et al* (2010) demonstrated that the mid-LV whole slice systolic circumferential strain, obtained from Duchenne muscular dystrophy patients with feature tracking, agreed well with harmonic phase imaging analysis. Subsequently the method was successfully applied to detect LV motion and strain during dobutamine stress (Schuster *et al* 2011). Augustine *et al* (2013) measured global and regional myocardial strains from cine CMR in 145 healthy volunteers with a feature tracking software. They found that the measured circumferential strain showed reasonable agreement with tagging measurement but not in longitudinal and radial strains. Feature tracking may fail due to inadequate local features for tracking and may not necessarily be accurate due to the limited information that is used. Deformable methods may overcome some of those limitations by incorporating information from a large image domain. Feng *et al* (2008) proposed a method based on b-spline non-rigid registration for computing 2D strains from cine CMR in both healthy volunteers and patients with myocardial infarction (MI), and they demonstrated that LV diastolic strain from cine images could be used to measure the changes in diastolic function in hypertensive patients.

However, there is a lack of information on the comparative accuracy of cine strain analysis with deformable methods and *in vivo* measurements such as DENSE, especially in patients with heart disease.

In this study, we developed a b-spline deformable method for estimating 2D strains (circumferential and radial strains) from short-axis cine CMR images in three healthy volunteers and 41 patients with either recent or chronic MI. Strain derived from cine CMR and its patterns were compared with DENSE, including the relationships between strain patterns and the transmural extent of scar and recovery time. This is the first direct comparison between cine CMR and DENSE on estimating 2D strains in both healthy volunteers and patients with MI. DENSE has a high degree of accuracy but also some limitations (Wen *et al* 2008), while cine CMR is routinely available. Therefore, we were interested in assessing whether or not LV strain estimated directly from cine CMR can be used to discriminate viable from non-viable myocardium as compared with DENSE.

2. Methods

2.1. CMR image acquisition

CMR studies were performed on three healthy volunteers (all male, aged 22–41 years old) and 41 MI patients (age: 59 $\pm$ 10, male: 31, female: 10). The patients were grouped according to a history of recent (<10 days post-MI, 16 patients) or chronic MI (>3 months post-MI, 25 patients). The local ethics committee approved the study protocol and all participants gave written informed consent.

CMR scans were performed on a Siemens MAGNETOM Avanto (Erlangen, Germany) 1.5-Tesla scanner with an 8-element phased array cardiac surface coil. CMR protocols included breath-hold steady state free precession cine, displacement encoded with simulated echoes (DENSE) and late gadolinium enhancement (LGE) phase sensitive inversion recovery (PSIR) (Payne *et al* 2011). Cine, DENSE and LGE CMR scans were obtained at the same position and only short-axis scans were post-processed in this study.

Cine CMR: Breath-hold steady state free precession cine was performed for assessing LV structure and function. Typical imaging parameters were: TR: 3.3 ms, TE: 1.21 ms, matrix size: 256 $\times$ 144, FOV: 360 $\times$ 255 mm^2, slice thickness: 7 mm, flip angle: 70°, receiver bandwidth: 930 Hz pixel^{-1}, at least 25 phases per cardiac cycle.

DENSE CMR: A 2D cine DENSE pulse sequence with short-echo-train echo-planar imaging readout was performed to measure 2D in-plane displacement vectors in two orthogonal encoding directions during a breath-hold of 15–20 s. Typical imaging parameters were: TR: 15 ms, TE: 8 ms, matrix size: 128 $\times$ 48, FOV: 448 $\times$ 168 mm^2, slice thickness: 8 mm, flip angle: 6°, receiver bandwidth: 1300 Hz pixel^{-1}, displacement-encoding sensitivity: 0.72 radian mm^{-1}, 20 phases per cardiac cycle. The average of two acquisitions was used to suppress noise. In the healthy volunteer study, since strain analysis by DENSE may not be applicable to every short-axis scan due to limitations related to a thin myocardial wall or dynamic motion of the LV apex, 12 short-axis scans were available for strain analysis by DENSE and cine CMR. In the patient study, due to the long breath-hold time with DENSE scans, only one short-axis scan was available for each patient, usually at the mid-ventricular level.

Late gadolinium enhancement (LGE) CMR: Ten minutes after intravenous injection of 0.10 mmol kg^{-1} of gadoterate meglumine (Gd^{2+-}DOTA, Dotarem, Guebert SA), LGE imaging was performed with a segmented PSIR turbo fast low-angle shot (PSIR-FLASH) (Kellman *et al* 2002). Typical imaging parameters were: TR: 8.7 ms, TE: 3.36 ms matrix size: 156 $\times$ 256,

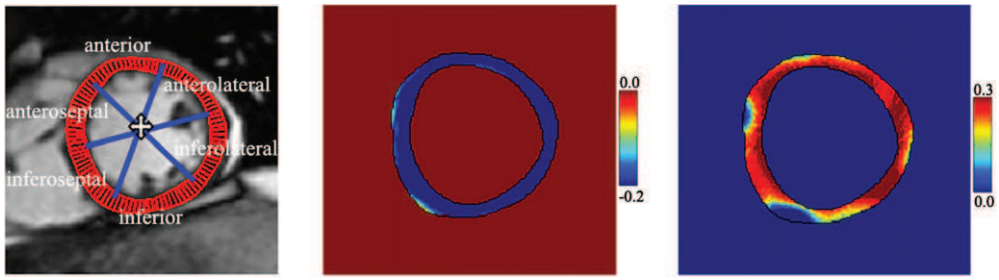

Figure 1. Strain estimation from the cine CMR images of a healthy volunteer: (a) Endocardial and epicardial boundaries with pre-defined six regions; (b) end-systolic circumferential strain map; (c) end-systolic radial strain map.

FOV: 292 × 360 mm^2, slice thickness: 8 mm, flip angle: 25°, receiver bandwidth: 130 Hz pixel^{-1}.

2.2. DENSE and LGE CMR image processing

DENSE images were post-processed by C.M. with DENSEView (National Institutes of Health, Bethesda, MD), a semi-automatic software that allows displacement maps and regional strain values to be obtained from DENSE CMR (Wen *et al* 2008). DENSE has been validated by different research groups, including in phantoms (Aletras *et al* 1999) and using tagged CMR as a reference standard for comparison (Kim *et al* 2004). LGE images were processed by an experienced cardiologist who was blind to the strain analysis. The MI scar score was reported for describing MI transmural extent as: 0: none, 1: 1%–25%, 2: 26%–50%, 3: 51%–75%, 4: 76%–100%, in which 0% represents unaffected myocardium, 100% represents totally non-viable myocardium. In this study, regional myocardial strain values from DENSE were used as reference standards to assess the accuracy of strain estimations from cine images. Each LV short-axis image was divided into six regions as anterior, anteroseptal, inferoseptal, inferior, inferolateral, and anterolateral (as shown in figure 1(a)).

2.3. Strain derived from cine CMR

Short-axis cine CMR images ($I_0, I_1, \ldots I_n$) were obtained at the same position as DENSE scans, and processed with an in-house code written in Matlab (The Mathworks, Natick, MA). The image which corresponds to the end-diastole (ED) cardiac phase was considered as the initial reference (I_0), the other phases (I_{cur}, cur $= 1, \ldots, j$) were registered back to the previous phase (I_{ref}, ref $= j - 1$) by using a b-spline deformable image registration method (Rueckert *et al* 1999) which minimizes the sum of squared differences between the two phases, defined as

$$\text{SSD} = \frac{1}{N}\sum_{i=1}^{N}\left(I_{\text{ref}}(p_i) - I_{\text{cur}}(p_i + T(p_i))\right)^2 \tag{1}$$

where N is the number of total pixels, I_{ref} is the reference image, I_{cur} is the current image for registration, p_i is the pixel position, and T is the inter-phase deformation transformation which is modelled with low resolution uniform cubic b-splines (compared to the image resolution) lying in the same image domain of I_{ref} ($\Omega = \{(x, y)|0 \leqslant x \leqslant X, 0 \leqslant y \leqslant Y\}$) ($X$, Y are the image size) with a uniform mesh of $n_x \times n_y$ control points, the displacement field associating

with the coarse mesh is denoted as $d_{J,K}$ $\left(0 \leqslant J < n_x; 0 \leqslant K < n_y\right)$, therefore for any position (x, y), the deformation field can be approximated by

$$T(x, y) = \sum_{l=0}^{3} \sum_{m=0}^{3} \beta_l(u)\beta_m(v)d_{J+l,K+m} \tag{2}$$

where $J = \text{integer}(x/h_x) - 1$, integer(.) operator is the integer part of x/h_x, $h_x = X/(n_x - 1)$, $u = x/h_x - J$, $K = \text{integer}(y/h_y) - 1$, $h_y = Y/(n_y - 1)$, $v = y/h_y - K$, and $\beta_l(u)$ represents the lth basis function of the cubic b-spline. The basic theory of b-spline deformable registration is that by manipulating the initial control points in the coarse mesh, the tentative solution of $d_{J,K}$ in those $n_x \times n_y$ control points is obtained from an optimization procedure by minimizing the squared difference of pixel intensities (equation (1)). The registration procedure was designed as $I_0 \leftarrow I_1 \leftarrow, \ldots \leftarrow I_n$ to cover a whole cardiac cycle.

In order to maintain the smoothness of the b-spline based transformation T, a penalty term was introduced to regularize T as

$$\text{Reg} = \frac{1}{A} \iint \frac{\partial^2 T}{\partial x^2} + 2\frac{\partial^2 T}{\partial xy} + \frac{\partial^2 T}{\partial y^2} \, \mathrm{d}x \, \mathrm{d}y \tag{3}$$

where A is the area of the image domain. Reg denotes the curvature of the coarse mesh and associates with the smoothness of T. The final solution of T was formulated as an optimization problem by minimizing a cost function C consisting of similarity measurement (SSD) and the regularization (Reg),

$$C = \text{SSD}(I_{\text{ref}}, T(I_{\text{cur}})) + \lambda \, \text{Reg}(T) \tag{4}$$

where λ represents the weighted or penalty parameter. The limited memory quasi-Newton Broyden–Fletcher–Goldfarb–Shanno method was used for the optimization procedure (Rueckert *et al* 1999).

Endocardial and epicardial boundaries were manually segmented in I_0, and then T was automatically calculated for all other phases, propagating from ED to end-systole (ES) and back to ED. The LV wall from cine image was also divided into six regions as shown in figure 1(a), which was consistent with DENSEView for circumferential and radial strain calculations. The 2D deformation gradient $\boldsymbol{F}$ is calculated as

$$\boldsymbol{F} = \begin{bmatrix} F_{11} & F_{12} \\ F_{21} & F_{22} \end{bmatrix} = \frac{\partial \boldsymbol{x}}{\partial \boldsymbol{X}} \tag{5}$$

where $\boldsymbol{x}$ denotes the position vector in I_{cur}, and $\boldsymbol{X}$ is the corresponding position vector in I_0. Then the finite strain tensor $\boldsymbol{E}$ at $\boldsymbol{X}$ is defined as

$$\boldsymbol{E} = \tfrac{1}{2}(\boldsymbol{F}^T\boldsymbol{F} - \boldsymbol{I}) \tag{6}$$

where $\boldsymbol{I}$ is the identity matrix. A rotation process was applied based on the LV shape centre for calculating circumferential and radial strains,

$$\boldsymbol{E}cr = \boldsymbol{R}^T\boldsymbol{E}R \tag{7}$$

where $\boldsymbol{R} = \begin{bmatrix} c_1 & r_1 \\ c_2 & r_2 \end{bmatrix}$; c $= [c_1 c_2]$ is the circumferential direction, r $= [r_1 r_2]$ is the radial direction, then Ecr(1, 1) is the circumferential strain and Ecr(2, 2) is the radial strain, their definitions were consistent with DENSEView. Figures 1(b), (c) shows an example of end-systolic circumferential and radial strains recovered from cine images. The end-systolic radial strain is less homogeneous compared to the circumferential strain. This difference may have resulted from the lack of local features for the b-spline deformable registration method to accurately recover the radial motions (such as the inferior insertion of the right ventricle to the left ventricle (figure 1(c)).

2.4. Strain estimation from the demons-based method

The demons deformable image registration method, proposed by Wang *et al* (2005), was implemented for strain estimation from the same short-axis cine CMR images of healthy volunteers to compare with the employed b-spline deformable method. The basic idea of demons is to determine a regular grid of forces which can deform the moving image I_{cur} into the fixed image I_{ref}. The demons force f is calculated from the optical flow equation, defined as

$$f = (I_{\text{cur}} - I_{\text{ref}}) \left(\frac{\nabla I_{\text{ref}}}{|\nabla I_{\text{ref}}|^2 + (I_{\text{ref}} - I_{\text{cur}})^2} + \frac{\nabla I_{\text{cur}}}{|\nabla I_{\text{cur}}|^2 + (I_{\text{ref}} - I_{\text{cur}})^2} \right) \tag{8}$$

∇ is the gradient operator. Equation (8) is solved iteratively, in each iteration, the deformation field is regularized by a Gaussian filter with a variance of σ^2. σ was chosen to be 3 based on 'trial and error'. Circumferential and radial strains from the demons method were calculated in the same way as the b-spline deformable method. Note that cine-derived strain in this study is referred to the b-spline derived strain from cine CMR, even though the demons method used same cine CMR images.

2.5. Statistical analysis

Peak circumferential and radial strains at pre-defined myocardial regions were identified at end-systolic phase from cine and DENSE, respectively. For each region, peak strain values were expressed as mean $\pm$ SD, and compared with the results from DENSE. The agreements were analysed by linear correlation analysis, Mann–Whitney *U*-test and Bland–Altman analysis. In the healthy volunteer study, except for the peak strain comparison, the strain curves from six pre-defined regions were also compared with the results from DENSE by using linear correlation analysis. Please refer to the appendix for the sample size calculation for the healthy volunteer study. In the patient study, peak strains were further compared with (1) recent and chronic MI states and (2) the transmural extent of MI. Receiver operating curve (ROC) of peak circumferential and radial strains derived from cine CMR images by using the b-spline deformable method and DENSE were performed for the distinction of (1) myocardial regions with MI from regions without MI, and (2) myocardial regions with transmural MI and regions with non-transmural MI. Statistical analysis was performed using Matlab (The Mathworks, Natick, MA), a probability value <0.05 was taken as statistically significant.

3. Results

3.1. Strain comparison in healthy volunteers

Figure 2 shows an example of myocardial strain estimations in six regions at a mid-ventricular short-axis level. The first row shows that the b-spline deformable method is able to track the motion of LV wall from ED to ES and back to late diastole. The second and third rows show the circumferential and radial strain curves estimated from cine and DENSE. Generally the trends of circumferential and radial strains estimated from DENSE have been well captured from the corresponding cine images with the b-spline deformable image registration method. The average linear correlation coefficients for the six-paired curves were 0.94 ± 0.02 for circumferential strain, 0.93 ± 0.06 for radial strain, and both were highly correlated ($p < 0.05$ *for all comparisons*). The average absolute circumferential strain difference was 0.02 ± 0.01 in one cardiac cycle; the difference for the radial strain was greater than the circumferential strain, which was 0.2 ± 0.015. Some time lag between cine and DENSE derived strain curves

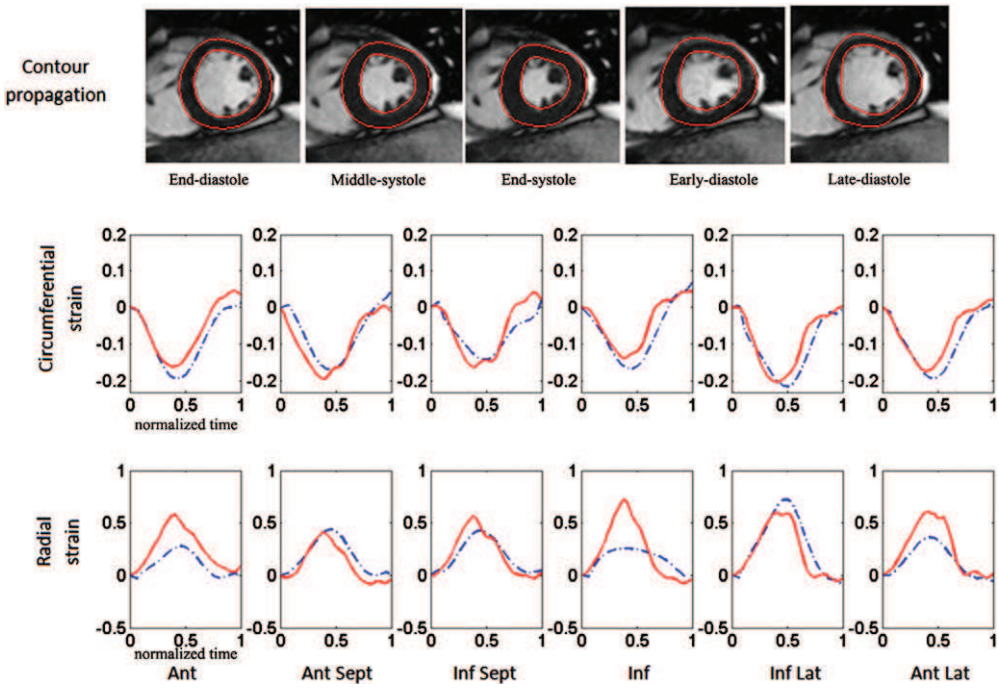

Figure 2. An example of strain estimation from the cine CMR images (solid) of a healthy volunteer compared with DENSE (dashed). The first row illustrates the LV wall motion tracked by the b-spline deformable model, enclosed by the endocardial and epicardial boundaries; the second row is the time course of circumferential strain estimated from cine (solid) and DENSE (dashed) scans; the third row is the time course of radial strain estimated from cine (solid) and DENSE (dashed) scans.

occurred which might be due to use of different phases in the DENSE acquisition. The similarity measurement by linear correlation analysis showed that, in 71 out of 72 regions from 12 short-axis scans, the cine-derived circumferential strain curves were significantly correlated with those from DENSE ($p < 0.05$ *for all comparisons*), with an averaged correlation coefficient of 0.88; radial strain curves from 67 out of 72 regions were correlated ($r = 0.87$, $p < 0.05$ *for all comparisons*).

The comparisons for peak circumferential and radial strains between cine and DENSE CMR are shown in figure 3. There was no difference in peak circumferential strain between cine and DENSE ($p = 0.76$) with a zero mean bias (figures 3(a), (c)). However peak radial strain differed when estimated by cine versus DENSE ($p < 0.01$) (figure 3(b)). The peak radial strain estimated from cine was higher than the strain values measured with DENSE, mean bias of 0.35 (figure 3(d)), suggesting that the b-spline deformable model overestimated peak radial strain in healthy LV.

3.2. Strain comparison in patients with MI

Figure 4 shows an example of an end-systolic LV strain map from a patient who underwent CMR two days after an anteroseptal MI. Figure 4(a) is the LGE CMR image, showing transmural MI in the anterior region (MI score 4) and non-transmural MI in the anteroseptal region (MI score 1). Figures 4(b), (c) shows the end-systolic circumferential and radial strain maps, respectively. In this example, there is close spatial correspondence between the observed

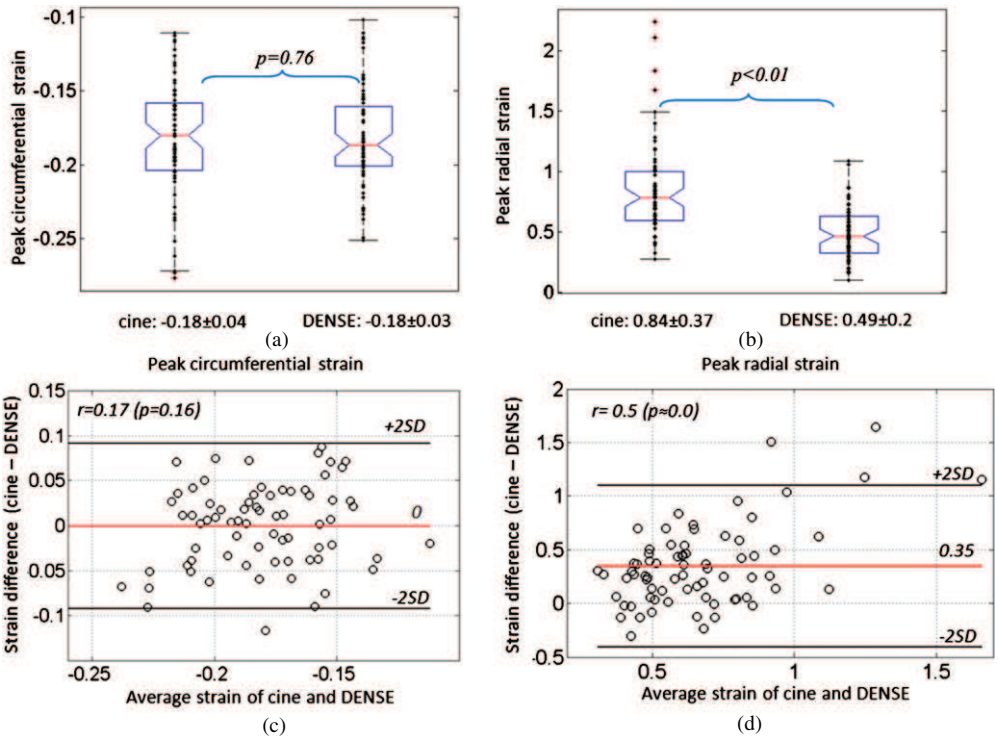

Figure 3. Myocardial strain comparisons for the three healthy volunteers: peak circumferential (a) and peak radial strain (b) comparison between cine and DENSE approaches, Bland–Altman analysis for peak circumferential strain (c) and peak radial strain (d).

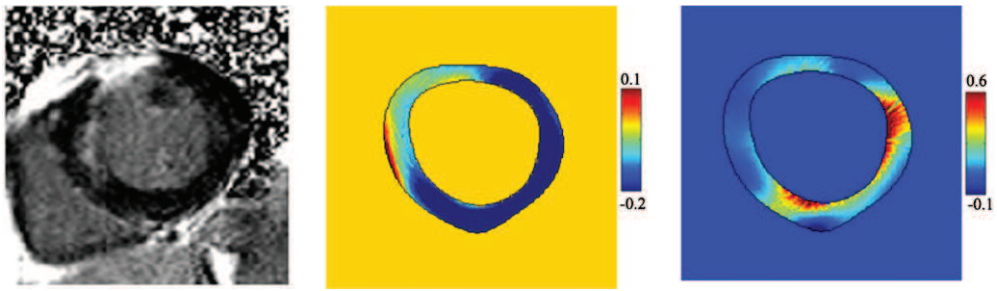

Figure 4. A left ventricular end-systolic strain maps computed from the cine CMR scans of a patient two days after an acute anterior transmural MI: (a) transmural MI in the anterior region delineated with late gadolinium enhancement CMR (MI score: 4) and non-transmural MI in the anteroseptal region (MI score: 1); (b) a co-registered end-systolic circumferential strain map and end-systolic radial strain map (c).

reductions in end-systolic strain and the distribution of LGE in the MI regions (circumferential strain (figure 4(b)): red equates to lower strain, blue to higher strain with negative value, reflecting fiber shortening and contraction; radial strain (figure 4(c)): red equates to higher strain with a positive value, indicating wall thickening, blue to lower strain).

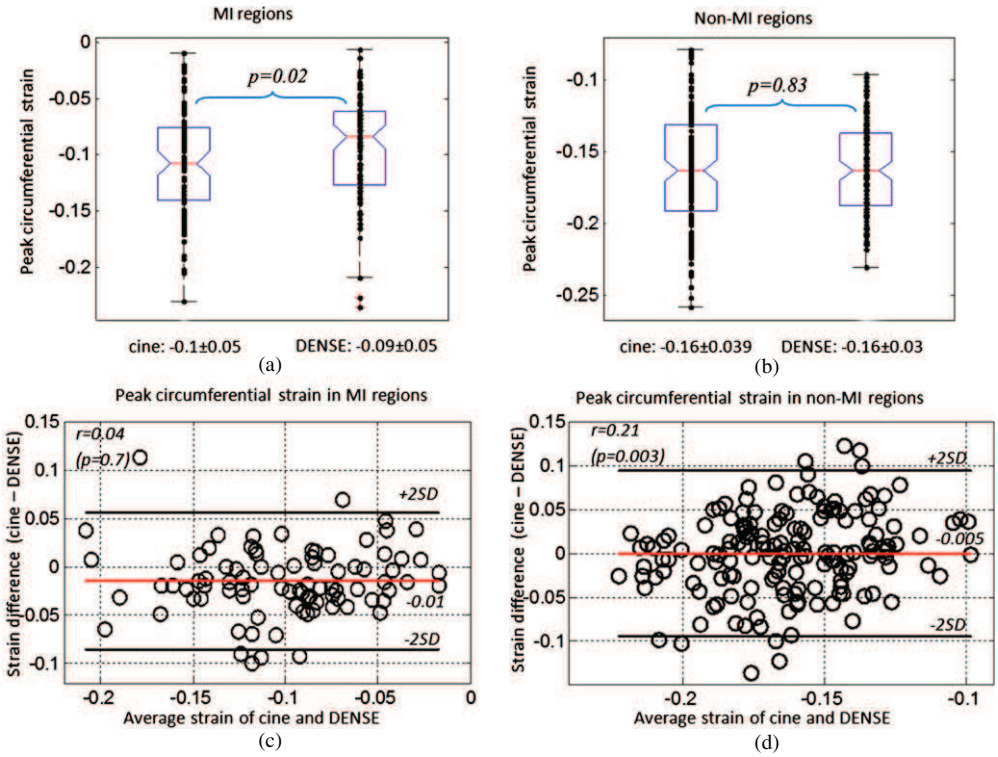

Figure 5. Peak circumferential strain comparison for regions-of-interest in the infarct zone (MI regions: $n = 88$) (a) and remote zones (non-MI regions: $n = 158$) (b), and the corresponding Bland–Altman analysis at MI regions (c) and non-MI regions (d) from the 41 patients.

Peak circumferential strain. Figures 5(a), (b) shows the comparison of peak circumferential LV strain estimated from cine and DENSE between MI and non-MI regions for all 41 MI patients. Overall, peak circumferential strain was similar when estimated by cine and DENSE although a small difference was observed for strain measured in MI regions ($p = 0.02$). Peak circumferential strain from both cine and DENSE had a lower value in MI regions (figure 5(a)) than in non-MI regions (figure 5(b)). Figures 5(c), (d) is the Bland–Altman plots for peak circumferential strain in MI and non-MI regions. A weak and positive correlation existed between the mean measured peak circumferential strain and its difference in non-MI region with $r = 0.21$ ($p = 0.003$), indicating that peak circumferential strain measured from cine images was slightly smaller than the value from DENSE when true strain was small, and higher when true strain was greater.

Peak radial strain. Figures 6(a), (b) shows peak radial strain comparisons between MI and non-MI regions. Peak circumferential and radial strains were lower in MI region compared to non-MI regions. Peak radial strain estimated by cine and DENSE had closer agreement in MI regions than in non-MI regions, however peak radial strain from cine was higher than strain derived from DENSE ($p < 0.01$) in non-MI regions. This over-estimation also existed in the healthy volunteer study as shown in figure 3(b). Figures 6(c), (d) shows the Bland–Altman plots for peak radial strain in MI and non-MI regions, greater agreement existed in MI regions than non-MI regions, associated with a larger mean bias (0.2). Overall, peak radial strain patterns estimated from cine agreed with strains measured from DENSE.

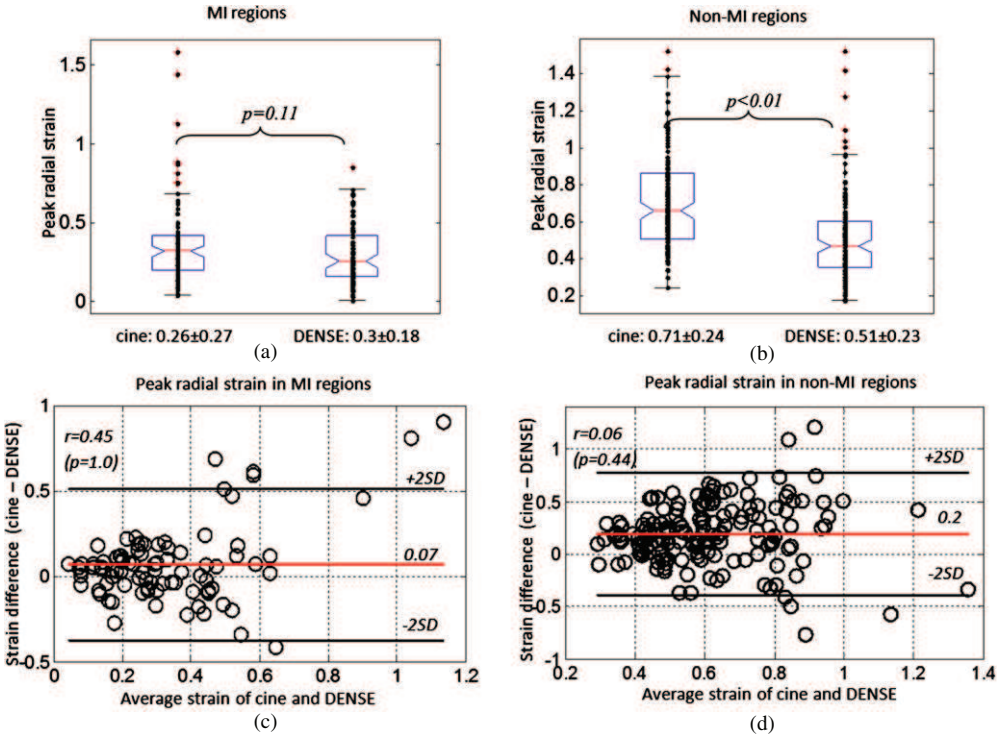

Figure 6. Peak radial strain comparison for regions-of-interest in the infarct zone (MI regions: $n = 88$) (a) and remote zones (non-MI regions: $n = 158$) (b), and the corresponding Bland–Altman analysis at MI regions (c) and non-MI regions (d) from the 41 patients.

Peak strain versus patients' recovery time and MI degree. Peak circumferential strains between the recent and chronic MI patient groups are shown in figure 7(a). For both groups, there was no difference between cine CMR and DENSE derived strain. Strain values in MI regions from the acute group were: -0.087 ± 0.04 from cine, -0.07 ± 0.04 from DENSE, consistent with a loss of contractility in acute MI. After three months follow up, peak circumferential strain at MI regions increased to -0.12 ± 0.05 (cine)/-0.11 ± 0.05 (DENSE). However peak circumferential strain at non-MI regions after three months had not changed (recent group: -0.16 ± 0.04 (cine), -0.16 ± 0.03 (DENSE) versus chronic group: -0.17 ± 0.04 (cine), -0.166 ± 0.03 (DENSE)). Figure 7(b) shows peak radial strain between the recent and chronic groups, and similar results were observed as with peak circumferential strain.

Figure 8 shows the relationship between peak strains in MI regions and MI transmural extent. Peak strains from cine and DENSE showed very close correspondence and decreased as the transmural extent of MI increased from MI score 1 to 4.

Distinction of MI and non-MI regions. From figures 5 and 6, non-MI and MI regions could be distinguished using peak circumferential and radial strains, shown in table 1 and figure 9. Figure 9(a) is the performance of peak circumferential strain for detecting non-MI and MI regions. The area under the curve (AUC) was 0.80 (95% confidence interval (CI): 0.74–0.86) for cine-derived circumferential strain, slightly lower than DENSE derived circumferential strain (AUC 0.88, 95% CI: 0.84–0.93). Figure 9(b) is the performance of peak radial strain

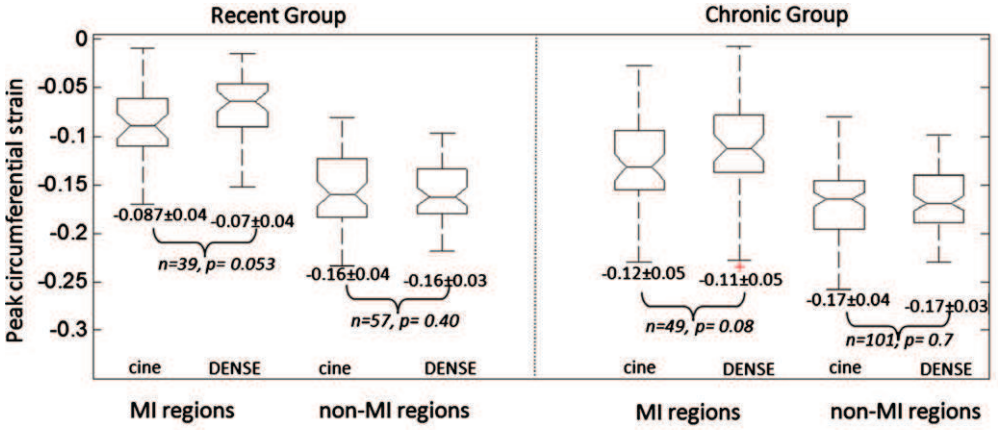

(a)

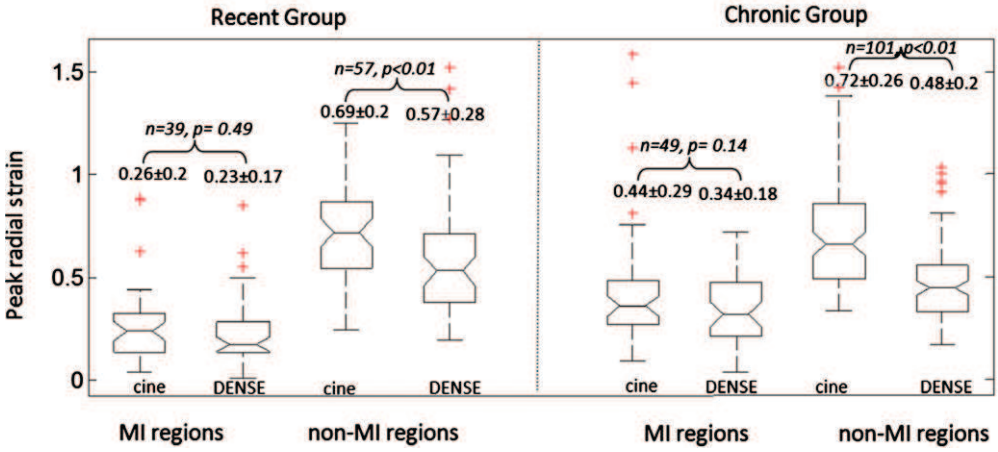

(b)

Figure 7. Myocardial strain in patients with either recent or chronic MI for (a) peak circumferential and (b) radial strains in MI and remote (non-MI) regions respectively, along with average values and box plots. Mann–Whitney *U*-test is used to determine the significance of a difference, n is the number of regions.

Table 1. Accuracy of peak circumferential and radial strains from cine CMR and DENSE for detection of myocardial regions with and without MI.

	Circumferential (cine)	Circumferential (DENSE)	Radial (cine)	Radial (DENSE)
Sensitivity	0.77	0.81	0.82	0.67
Specificity	0.71	0.79	0.88	0.81
Cut-off value	−0.14	−0.13	0.44	0.32
AUC	0.80	0.88	0.87	0.78
95% CI	0.74–0.86	0.84–0.93	0.83–0.93	0.72–0.83

AUC: area under curve; CI: confidence interval.

for detecting non-MI and MI regions, the AUC for cine-derived radial strain was 0.87 (95% CI: 0.83–0.93), higher than DENSE derived radial strain (AUC: 0.78, 95% CI: 0.72–0.83). The higher performance for peak radial strain from cine CMR images could be due to the overestimation in non-MI regions, but not in MI regions (figures 6(a) and (b)). Overall, strains

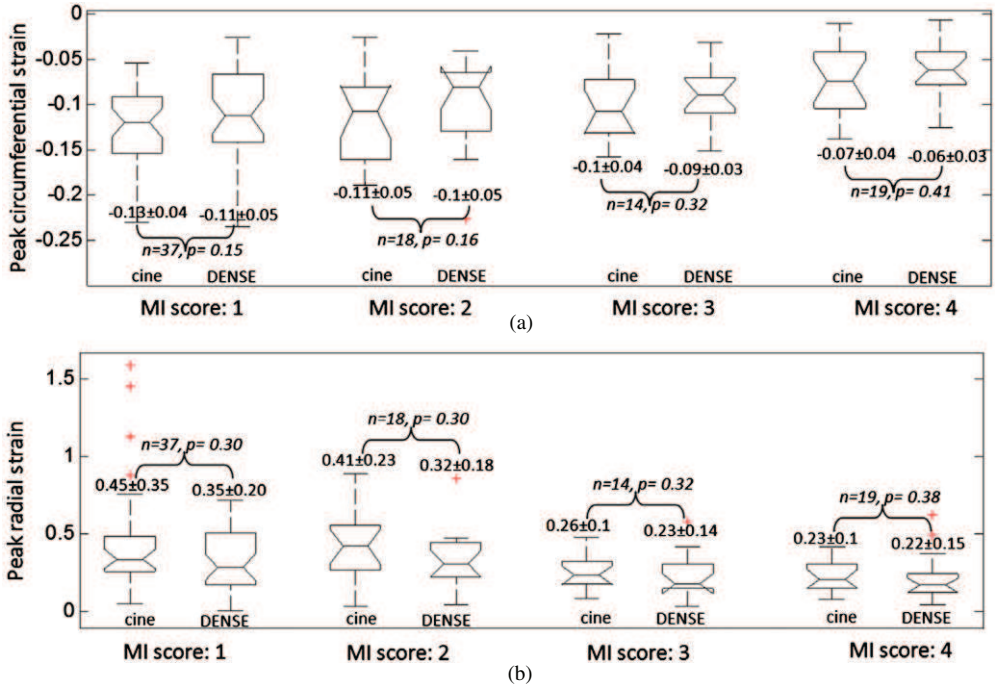

Figure 8. The relationship between peak strain values and different MI scores from 1 to 4: (a) peak circumferential strain; (b) peak radial strain, along with average values and box plots. Mann–Whitney *U*-test is used to determine the significance of a difference, n is the number of regions.

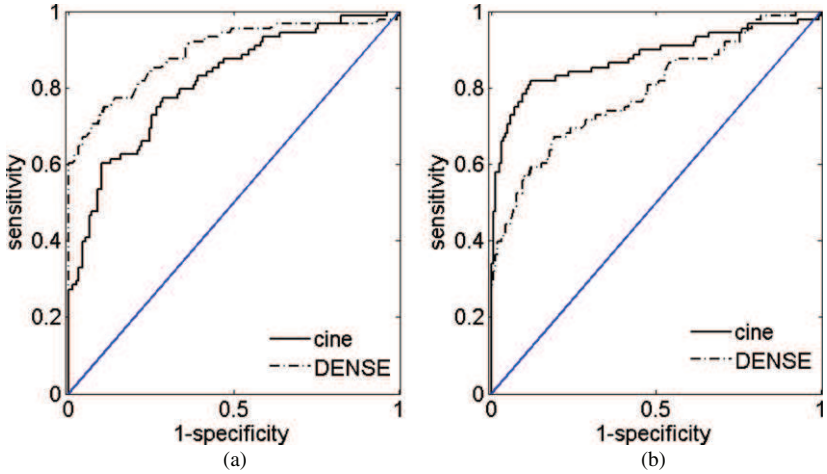

Figure 9. ROCs of peak circumferential (a) and radial (b) strains from cine CMR and DENSE for the distinction of MI and non-MI regions.

estimated from cine CMR images by the b-spline deformable method and from DENSE allowed discrimination between MI and non-MI regions with similar accuracy.

Distinction of non-transmural MI and transmural MI regions. According to the transmural score, MI regions were further divided into two groups as the non-transmural group with MI

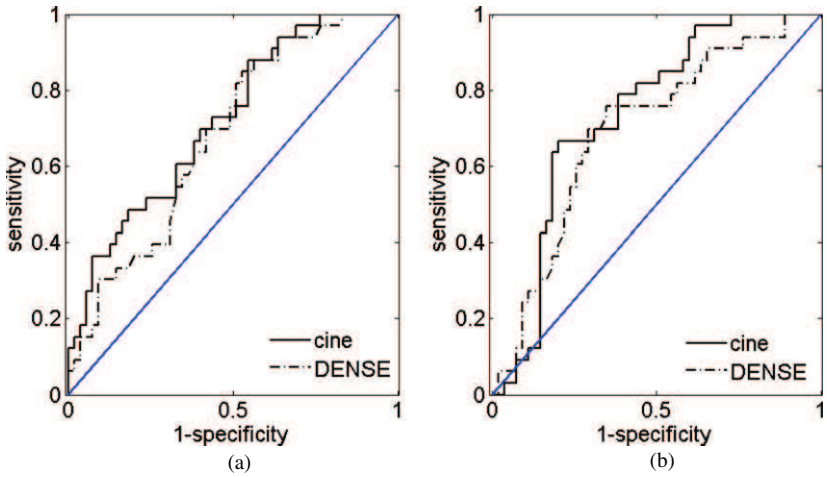

Figure 10. ROCs of peak circumferential (a) and radial (b) strains derived from cine CMR images and DENSE for the distinction of transmural and non-transmural MI regions.

Table 2. Accuracy of peak circumferential and radial strains from cine CMR images and DENSE for detection of myocardial regions with transmural and non-transmural MI.

	Circumferential (cine)	Circumferential (DENSE)	Radial (cine)	Radial (DENSE)
Sensitivity	0.70	0.70	0.67	0.70
Specificity	0.60	0.58	0.80	0.71
Cut-off value	−0.11	−0.09	0.26	0.24
AUC	0.70	0.66	0.72	0.70
95% CI	0.58–0.82	0.54–0.78	0.61–0.84	0.58–0.81

AUC: area under curve; CI: confidence interval.

scar extent less than 50% (MI scores 1 and 2) and the transmural group with MI scar extent higher than 50% (MI scores 3 and 4). The ROC analysis suggested that the transmural MI group could also be distinguished from the non-transmural MI group, shown in table 2 and figure 10. Figure 10(a) is the performance of peak circumferential strain derived from cine CMR images with AUC 0.70 (95% CI: 0.58–0.82), slightly higher than DENSE derived strain (AUC 0.66, 95% CI: 0.54–0.78). Similar results were found for peak radial strain (figure 10(b)).

3.3. Comparison with the demons method

Figure 11 shows an example of strains estimated from the implemented demons method (dotted), compared with the b-spline method (solid) and DENSE results (dashed). Strains derived from the demons method were comparable to the strains estimated from the b-spline method and DENSE, but some discrepancies existed, such as an overestimation of peak radial strain, as shown in figure 11 (the bottom panel). The average peak circumferential strain for the three volunteers from the demons method was -0.165 ± 0.05, lower than the values from the b-spline method ($p = 0.04$) and DENSE ($p = 0.02$). The average peak radial strain was 1.25 ± 0.5, which was significantly higher than both values from the b-spline method and DENSE ($p < 0.01$).

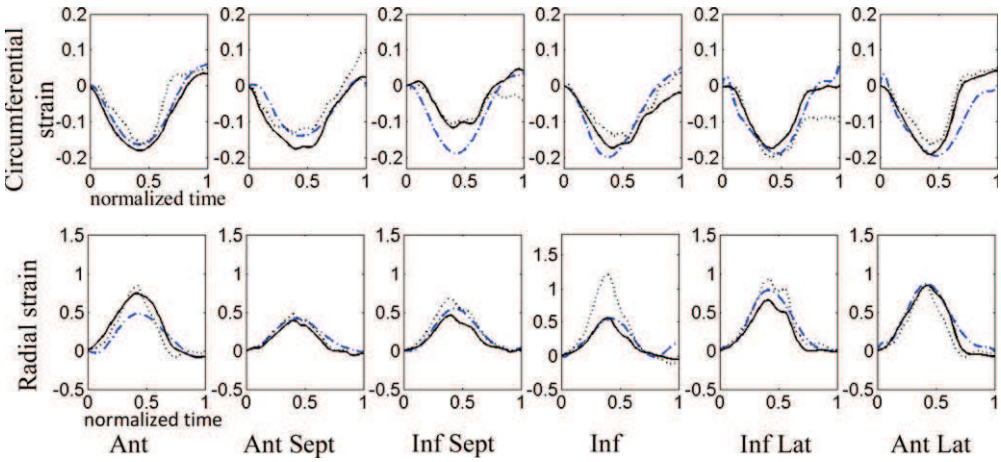

Figure 11. An example of myocardial strain estimation from the cine CMR images of a healthy volunteer by using the demons method (dotted), b-spline deformable method (solid), compared with DENSE results (dashed). The first row is the time course of circumferential strains in the pre-defined six regions; the second row is the time course of radial strains.

4. Discussion

The clinical significance of heart disease can only be fully appreciated with knowledge of myocardial function. Accordingly, myocardial strain is more informative about contractility than displacement and motion (Gotte *et al* 2001). Furthermore, myocardial strain is a stronger predictor of survival than LV ejection fraction which is typically derived by measurement of LV wall motion (Stanton *et al* 2009). Strain CMR and related image processing methods have been developed to estimate LV strains but these methods require additional scans, which may involve long breath-holds and may also prolong the CMR scan duration. In this study, myocardial strain was estimated from conventional cine CMR by using a b-spline deformable image registration method, and the results were validated with DENSE derived strain from healthy volunteers and patient datasets. Our results are clinically relevant since our findings suggest that strain could be estimated from standard cine scans without the need for extra strain-specific breath-hold scans.

In the healthy volunteer study, circumferential strains estimated from cine agreed well with those from DENSE with negligible bias for peak values from Bland–Altman analysis, but with a more dispersed range and slightly higher average value (-0.18 ± 0.04). Peak circumferential strains from cine CMR were comparable to the ranges reported by Moore *et al* (2000), around -0.2, Nasiraei *et al* (Nasiraei Moghaddam *et al* 2010), around -0.18, and Augustine *et al* (2013), around -0.18. Radial strains estimated from cine CMR were not as good as circumferential strains when compared with DENSE, and similar results have been reported by Augustine *et al* (2013). The average peak radial strain in our study was higher than DENSE derived values, and also higher than the ranges from Moore *et al*'s study, around 0.44 for septal wall and lateral wall, and from Nasiraei *et al*'s study, around 0.54. The reason for the greater agreement in circumferential strains with other studies might relate to myofibre orientation which is more homogeneous in the circumferential direction than in the radial direction (Waldman *et al* 1985), which means that circumferential strain is more homogeneous. The strain estimation can be improved by incorporating myofiber orientation

in the developed b-spline deformable method. In the current implementation, for a short-axis scan with 35 phases in one cardiac cycle, it takes around 5 min using the MATLAB. The computational time can be significantly reduced by using more efficient solvers in future.

In figures 5 and 6, peak strains in the MI regions were much lower than the non-MI regions from both cine and DENSE derived values. From the corresponding ROC analysis, the differences between the peak circumferential and radial strains in the MI and non-MI regions could provide a way to assess abnormalities in regional myocardial function. The accuracy of distinction of regions with MI from regions without MI by using cine-derived strains was comparable to DENSE derived strains (table 1). After acute MI, myocardial contractility is impaired in the affected regions. However, contractility may improve over time under the favourable influence of endogenous healing, coronary collateral blood flow and secondary prevention therapies. In our study, both peak circumferential and radial strains in MI regions were greater in the chronic MI group compared to the recent MI group, and our findings are consistent with those of Antoni *et al* (2010) and Pahlm-Webb *et al* (2009). In figure 8, there was a progressive decrease in peak circumferential and radial strain values related to the transmural extent of the infarction, which is also consistent with previous findings (Sachdev *et al* 2006). The relationship between the decreased strain and MI transmural extent could also be used for distinguishing MI transmurality (Neizel *et al* 2009) by using cine-derived strains, which had similar accuracy as strains derived from DENSE (table 2).

In general, we have demonstrated that myocardial strain estimation from cine CMR using the b-spline deformable method could be an alternative option during clinical practice when strain CMR is not available (Phatak *et al* 2009), particularly for patients with difficulties in acquiring high quality strain CMR data. Our results indicate that peak circumferential strain derived from cine CMR would be the preferred option, and this fits well with prior clinical data supporting the diagnostic value of this circumferential strain for assessing myocardial viability (Soleimanifard *et al* 2012), and is being widely used (Altiok *et al* 2013, Becker *et al* 2009, Koos *et al* 2013). Although the peak radial strain was overestimated from the cine CMR for healthy volunteers and non-MI regions in patients, there was a high level of agreement for MI regions between cine-derived radial strain values and DENSE. Useful information could still be derived from peak radial strain patterns for myocardium viability assessment as shown in tables 1 and 2. We remark that the absolute value of peak radial strain estimated from the b-spline method needs to be interpreted with caution, especially for the viable myocardium, and should be used in conjunction with the circumferential strain.

Validation of deformable image registration methods is challenging and technical approaches may require implanted markers, or dedicated experiments, which may not feasible in clinical practice (Wierzbicki *et al* 2004). In this study, the cine-derived strains from the developed b-spline method were compared with DENSE. We also compared our method with the demons method (Wang *et al* 2005), which is based on grey-scale deformable registration. The comparison with demons deformable registration method with three healthy volunteer showed that the b-spline deformable method could estimate regional strains closer to DENSE. As suggested by Kashani *et al*, no deformable registration method can predict deformation uniformly accurate across all regions (Kashani *et al* 2008), therefore the closer strain estimation from the developed b-spline method requires a more rigorous evaluation.

The discrepancy between cine CMR and DENSE derived strains (especially the radial strains in healthy myocardium region) can be influenced by following factors. (1) The developed b-spline deformable image registration method depends on the intensity information for deforming the images; therefore it will be affected by image qualities. In the CMR scan, the patients and volunteers were asked to hold the breath to minimize the motions related to respiration, but small amount of respiratory motions still exist. This may contribute to the

uncertainties, which also exist in DENSE. (2) As reported in Wierzbicki's study (Wierzbicki *et al* 2004) and others (Kashani *et al* 2008), the non-rigid registration method can track boundaries, such as the epicardial surface, with reasonable resolution, but not so well within myocardium tissue because of limited contrast. This is the reason for the inhomogeneous estimated strains from cine CMR in figures 1(b) and (c). (3) The trabeculated myocardial layer can also contribute to measurement variability, especially for radial strain estimation. The reason for that is because the trabeculated myocardial layer attaches to the LV wall during diastole and then move markedly along the radial direction during systole. The large motions from the trabeculated myocardial layer can be interpolated into the LV wall by the b-spline deformable model (equation (2)). This fact may explain the much higher peak radial strain from cine images when compared to the values from DENSE. Furthermore, since there is generally greater noise with radial strain estimates with DENSE than with circumferential estimates (Wen *et al* 2008, Ibrahim el 2011), limitations with the DENSE reference method may also contribute to the lower agreement with radial strain.

Future works should focus on (1) maintaining the symmetry and inverse-consistency of the estimated deformation field in the employed b-spline deformable image registration method (Guetter *et al* 2011); (2) incorporating more features for accurate pixel-wise strain map estimation, such as curvature (Sinusas *et al* 2001), myocardium incompressibility (Bistoquet *et al* 2007); (3) 3D strain estimation from cine CMR; (4) finally our results should be examined in larger patient cohorts, including different cardiac conditions.

5. Conclusions

In this study, myocardial strain estimated from conventional cine CMR using b-spline deformable image registration technique was compared with DENSE, which served as a reference method. Our results showed that the peak circumferential and radial strains from cine images were comparable to the values from DENSE for both healthy volunteers and patients with MI. Cine-derived strain disclosed different strain patterns in MI and non-MI regions as was also the case with DENSE, and characterized myocardial viability with similar accuracy as DENSE. Large variations existed in radial strain estimates such that radial strain values were potentially inaccurate and might not be clinically useful. Overall, this work demonstrated that useful strain information can be obtained from routine cine CMR scans. From a clinical perspective, strain estimation from cine CMR may be most useful when strain CMR is not performed or available.

Acknowledgments

We would like to thank Peter Weale from Siemens Healthcare and Dr Han Wen, who provided the DENSE pulse sequence. We also would like to thank Dr Alex Payne for providing MI transmural extent, Professor Dirk Husmeier from the University of Glasgow for discussion on statistical analysis. We gratefully acknowledge funding support from the Medical Research Scotland, and the Engineering and Physical Sciences Research Council (grant no EP/I029990). The authors declare that they have no competing interests.

Appendix. Sample size calculation for the healthy volunteer study

There were 12 short-axis slices available for strain measurements by DENSE and cine CMR in the healthy volunteer study. Strain estimation with each method was compared based on six

pre-defined LV regions in each short-axis slice, which means that the total data set included 72 points rather than 3. If the estimated peak circumferential strain from cine CMR images is a normal distribution with a standard deviation σ no more than 0.05 and the margin error M is 0.02, then to achieve 95% confidence that the estimated circumferential strain is within a distance of M of the true mean, the minimum sample size for regional peak circumferential strain would be

$$n = 4\sigma^2/M^2 = 25 \text{ (data points)}.$$

For regional peak radial strain, as with the regional peak circumferential strain and assuming that strain follows a normal distribution with a standard deviation σ no more than 0.4 and the margin error M is 0.1, then to achieve 95% confidence that the estimated radial strain is within a distance of M of the true mean, the minimum sample size for regional peak radial strain would be

$$n = 4\sigma^2/M^2 = 64 \text{ (data points)}.$$

Although only three healthy volunteers were included for the healthy volunteer study and in fact the data points obtained from these three healthy volunteers (72) exceeded the required minimum sample sizes.

References

Aletras A H, Ding S, Balaban R S and Wen H 1999 DENSE: displacement encoding with stimulated echoes in cardiac functional MRI *J. Magn. Reson.* **137** 247–52

Aletras A H, Tilak G S, Hsu L Y and Arai A E 2011 Heterogeneity of intramural function in hypertrophic cardiomyopathy: mechanistic insights from MRI late gadolinium enhancement and high-resolution displacement encoding with stimulated echoes strain maps *Circ. Cardiovasc. Imaging* **4** 425–34

Altiok E *et al* 2013 Layer-specific analysis of myocardial deformation for assessment of infarct transmurality: comparison of strain-encoded cardiovascular magnetic resonance with 2D speckle tracking echocardiography *Eur. Heart J. Cardiovasc. Imaging* **14** 570–8

Antoni M L, Mollema S A, Atary J Z, Borleffs C J, Boersma E, Van de Veire N R, Holman E R, Van der Wall E E, Schalij M J and Bax J J 2010 Time course of global left ventricular strain after acute myocardial infarction *Eur. Heart J.* **31** 2006–13

Augustine D *et al* 2013 Global and regional left ventricular myocardial deformation measures by magnetic resonance feature tracking in healthy volunteers: comparison with tagging and relevance of gender *J. Cardiovasc. Magn. Reson.* **15** 8

Becker M *et al* 2009 Impact of infarct transmurality on layer-specific impairment of myocardial function: a myocardial deformation imaging study *Eur. Heart J.* **30** 1467–76

Berry C, Kellman P, Mancini C, Chen M Y, Bandettini W P, Lowrey T, Hsu L Y, Aletras A H and Arai A E 2010 Magnetic resonance imaging delineates the ischemic area at risk and myocardial salvage in patients with acute myocardial infarction *Circ. Cardiovasc. Imaging* **3** 527–35

Bistoquet A, Oshinski J and Skrinjar O 2007 Left ventricular deformation recovery from cine MRI using an incompressible model *IEEE Trans. Med. Imaging* **26** 1136–53

Castillo E, Lima J A and Bluemke D A 2003 Regional myocardial function: advances in MR imaging and analysis *Radiographics* **23** Spec no: S127–40

Conti C A, Votta E, Corsi C, De Marchi D, Tarroni G, Stevanella M, Lombardi M, Parodi O, Caiani E G and Redaelli A 2011 Left ventricular modelling: a quantitative functional assessment tool based on cardiac magnetic resonance imaging *Interface Focus* **1** 384–95

Feng W, Denney T S, Lloyd S, Dell'italia L and Gupta H 2008 Contour regularized left ventricular strain analysis from cine MRI *ISBI'08: 5th IEEE Int. Symp. on Biomedical Imaging: From Nano to Macro (14–17 May 2008)* pp 520–3

Gotte M J, Van Rossum A C, Twisk J W R, Kuijer J P A, Marcus J T and Visser C A 2001 Quantification of regional contractile function after infarction: strain analysis superior to wall thickening analysis in discriminating infarct from remote myocardium *J. Am. College Cardiol.* **37** 808–17

Guetter C, Hui X, Chefd'hotel C and Guehring J 2011 Efficient symmetric and inverse-consistent deformable registration through interleaved optimization *IEEE Int. Symp. on Biomedical Imaging: From Nano to Macro (30 March–2 April 2011)* pp 590–3

Hor K N, Gottliebson W M, Carson C, Wash E, Cnota J, Fleck R, Wansapura J, Klimeczek P, Al-Khalidi H R and Chung E S 2010 Comparison of magnetic resonance feature tracking for strain calculation with harmonic phase imaging analysis *JACC: Cardiovasc. Imaging* **3** 144–51

Ibrahim el S H 2011 Myocardial tagging by cardiovascular magnetic resonance: evolution of techniques–pulse sequences, analysis algorithms, and applications *J. Cardiovasc. Magn. Reson.* **13** 36

Isbell D C and Kramer C M 2005 Cardiovascular magnetic resonance: structure, function, perfusion, and viability *J. Nucl. Cardiol.* **12** 324–36

Jung B, Zaitsev M, Hennig J and Markl M 2006 Navigator gated high temporal resolution tissue phase mapping of myocardial motion *Magn. Reson. Med.* **55** 937–42

Kashani R *et al* 2008 Objective assessment of deformable image registration in radiotherapy: a multi-institution study *Med. Phys.* **35** 5944–53

Kellman P, Arai A E, Mcveigh E R and Aletras A H 2002 Phase-sensitive inversion recovery for detecting myocardial infarction using gadolinium-delayed hyperenhancement *Magn. Reson. Med.* **47** 372–83

Kim D, Gilson W D, Kramer C M and Epstein F H 2004 Myocardial tissue tracking with two-dimensional cine displacement-encoded MR imaging: development and initial evaluation *Radiology* **230** 862–71

Kim D and Kellman P 2007 Improved cine displacement-encoded MRI using balanced steady-state free precession and time-adaptive sensitivity encoding parallel imaging at 3 T *NMR Biomed.* **20** 591–601

Koos R, Altiok E, Doetsch J, Neizel M, Krombach G, Marx N and Hoffmann R 2013 Layer-specific strain-encoded MRI for the evaluation of left ventricular function and infarct transmurality in patients with chronic coronary artery disease *Int. J. Cardiol.* **166** 85–9

Leitman M, Lysyansky P, Sidenko S, Shir V, Peleg E, Binenbaum M, Kaluski E, Krakover R and Vered Z 2004 Two-dimensional strain-a novel software for real-time quantitative echocardiographic assessment of myocardial function *J. Am. Soc. Echocardiogr.* **17** 1021–9

Li J and Denney T S Jr 2006 Left ventricular motion reconstruction with a prolate spheroidal B-spline model *Phys. Med. Biol.* **51** 517–37

Mansi T, Peyrat J M, Sermesant M, Delingette H, Blanc J, Boudjemline Y and Ayache N 2009 Physically-constrained diffeomorphic demons for the estimation of 3d myocardium strain from cine-MRI *Funct. Imaging Model. Heart* **5528** 201–10

Moore C C, Lugo-Olivieri C H, Mcveigh E R and Zerhouni E A 2000 Three-dimensional systolic strain patterns in the normal human left ventricle: characterization with tagged MR imaging *Radiology* **214** 453–66

Nasiraei Moghaddam A, Saber N R, Wen H, Finn J P, Ennis D B and Gharib M 2010 Analytical method to measure three-dimensional strain patterns in the left ventricle from single slice displacement data *J. Cardiovasc. Magn. Reson.* **12** 33

Neizel M, Lossnitzer D, Korosoglou G, Schaufele T, Peykarjou H, Steen H, Ocklenburg C, Giannitsis E, Katus H A and Osman N F 2009 Strain-encoded MRI for evaluation of left ventricular function and transmurality in acute myocardial infarction *Circ. Cardiovasc. Imaging* **2** 116–22

Osman N F, Sampath S, Atalar E and Prince J L 2001 Imaging longitudinal cardiac strain on short-axis images using strain-encoded MRI *Magn. Reson. Med.* **46** 324–34

Pahlm-Webb U, Heiberg E, Hedstrom E and Arheden H 2009 Evolution of left ventricular strain after a first time myocardial infarction. A study using velocity encoded magnetic resonance imaging *J. Cardiovasc. Magn. Reson.* **11** P268

Papademetris X, Sinusas A J, Dione D P, Constable R T and Duncan J S 2002 Estimation of 3D left ventricular deformation from medical images using biomechanical models *IEEE Trans. Med. Imaging* **21** 786–800

Payne A R *et al* 2011 Bright blood T2 weighted MRI has higher diagnostic accuracy than dark blood STIR MRI for detection of acute myocardial infarction and for assessment of the ischemic area-at-risk and myocardial salvage *Circ. Cardiovasc. Imaging* **4** 210–9

Phatak N S, Maas S A, Veress A I, Pack N A, Di Bella E V and Weiss J A 2009 Strain measurement in the left ventricle during systole with deformable image registration *Med. Image Anal.* **13** 354–61

Rueckert D, Sonoda L I, Hayes C, Hill D L, Leach M O and Hawkes D J 1999 Nonrigid registration using free-form deformations: application to breast MR images *IEEE Trans. Med. Imaging* **18** 712–21

Sachdev V *et al* 2006 Myocardial strain decreases with increasing transmurality of infarction: a Doppler echocardiographic and magnetic resonance correlation study *J. Am. Soc. Echocardiogr.* **19** 34–9

Schuster A, Kutty S, Padiyath A, Parish V, Gribben P, Danford D A, Makowski M R, Bigalke B, Beerbaum P and Nagel E 2011 Cardiovascular magnetic resonance myocardial feature tracking detects quantitative wall motion during dobutamine stress *J. Cardiovasc. Magn. Reson.* **13** 58

Shi Z, Yue M, Gang W and Yubei G 2009 Left ventricular strain analysis from cine MRI *BMEI '09: 2nd Int. Conf. on Biomedical Engineering and Informatics (17–19, Oct. 2009)* pp 1–5

Sinusas A J, Papademetris X, Constable R T, Dione D P, Slade M D, Shi P and Duncan J S 2001 Quantification of 3D regional myocardial deformation: shape-based analysis of magnetic resonance images *Am. J. Physiol. Heart Circ. Physiol.* **281** H698–714

Soleimanifard S, Abd-Elmoniem K Z, Sasano T, Agarwal H K, Abraham M R, Abraham T P and Prince J L 2012 Three-dimensional regional strain analysis in porcine myocardial infarction: a 3T magnetic resonance tagging study *J. Cardiovasc. Magn. Reson.* **14** 85

Stanton T, Ingul C B, Hare J L, Leano R and Marwick T H 2009 Association of myocardial deformation with mortality independent of myocardial ischemia and left ventricular hypertrophy *JACC: Cardiovasc. Imaging* **2** 793–801

Veress A I, Gullberg G T and Weiss J A 2005 Measurement of strain in the left ventricle during diastole with cine-MRI and deformable image registration *J. Biomech. Eng.* **127** 1195–207

Waldman L K, Fung Y C and Covell J W 1985 Transmural myocardial deformation in the canine left ventricle. Normal *in vivo* three-dimensional finite strains *Circ. Res.* **57** 152–63

Wang H, Dong L, O'daniel J, Mohan R, Garden A S, Ang K K, Kuban D A, Bonnen M, Chang J Y and Cheung R 2005 Validation of an accelerated 'demons' algorithm for deformable image registration in radiation therapy *Phys. Med. Biol.* **50** 2887–905

Wen H, Marsolo K A, Bennett E E, Kutten K S, Lewis R P, Lipps D B, Epstein N D, Plehn J F and Croisille P 2008 Adaptive postprocessing techniques for myocardial tissue tracking with displacement-encoded MR imaging *Radiology* **246** 229–40

Wierzbicki M, Drangova M, Guiraudon G and Peters T 2004 Validation of dynamic heart models obtained using non-linear registration for virtual reality training, planning, and guidance of minimally invasive cardiac surgeries *Med. Image Anal.* **8** 387–401

Xu C, Pilla J J, Isaac G, Gorman J H 3rd, Blom A S, Gorman R C, Ling Z and Dougherty L 2010 Deformation analysis of 3D tagged cardiac images using an optical flow method *J. Cardiovasc. Magn. Reson.* **12** 19

Zerhouni E A, Parish D M, Rogers W J, Yang A and Shapiro E P 1988 Human heart: tagging with MR imaging–a method for noninvasive assessment of myocardial motion *Radiology* **169** 59–63 (PMID: 3420283)